East European Journal of Physics. 4. 284-290 (2025)
DOI:10.26565/2312-4334-2025-4-26 ISSN 2312-4334

NUMERICAL INVESTIGATION OF LEAD-FREE PEROVSKITE SOLAR CELLS BASED ON $FASnI_3/ZrS_2$ STRUCTURE USING SCAPS-1D SIMULATOR

Hmoud Al-Dmour
Mutah University, Faculty of Science, Department of Physics, 61710, Jordan
Corresponding Author E-mail: hmoud79@mutah.edu.jo
Received August 8, 2025; revised September 28, 2025; accepted October 9, 2025

This study presents a numerical investigation and optimization of lead-free perovskite solar cells using SCAPS-1D simulation. The proposed device is composed of formamidinium tin iodide ($FASnI_3$, absorptive layer), zirconium disulfide (ZrS_2, electron transport material), gold (Au, the back contact), and Fluorine-doped tin oxide (SnO_2:F, the front contact).The effects of varying the thickness, defect density, doping concentration, operating temperature, and back-contact work function on the photovoltaic performance were studied to determine the optimal device architecture with the highest power conversion efficiency (PCE). Results reveal that the initial performance of $FASnI_3/ZrS_2$ solar cells was as follows: open-circuit voltage (V_{OC}) =0.99V, short-circuit current (J_{SC}) = 20.7mA/cm^2, Fill factor (FF) = 60.13%, and power conversion efficiency (PCE)=12.4%.After optimization, the performance of $FASnI_3/ZrS_2$ significantly improved, achieving a PCE of 23.3%, FF of 82.4%, and J_{SC} of 30.2mA/cm^2.This remarkable improvement in these parameters is attributed to the increase in thickness and doping density of the $FASnI_3$ and ZrS_2 layers which lead to improved light absorption and charge generation. Additionally, the 5.3 eV work function of the back contact was found to provide better energy-level alignment with the $FASnI_3$ layer, thereby facilitating charge extraction. These findings offer valuable insights into the design of efficient, stable, and lead-free perovskite solar cells.
Keywords: *$FASnI_3$; ZrS_2; SCAPS-1D; Lead-free perovskite solar cells; Electron transport layer; Photovoltaic modeling; Solar energy*
PACS: 28.41.Ak, 88.40.H, 61.72.Vv,71.55.−I, 73.30.+

1. INTRODUCTION

Over the last decade, human demand for energy has increased due to our growing reliance on technology, resulting in a corresponding rise in the use of fossil fuels [1]. They are non-renewable and take a long time to form. Additionally, burning fossil fuels releases CO_2 gas, which accumulates in the atmosphere [1]. Thus, considerable efforts have been made to replace fossil fuels with renewable energy sources, such as solar and nuclear energy. Solar energy is produced using solar cells, which offer a promising renewable energy source, providing an environmentally friendly way to curb CO_2 emissions and meet the growing demand for green energy [1.2]. This has led to an increasing demand for ecologically friendly photovoltaic devices, such as tin-based perovskite solar cells (PSCs) [2,3]. They have been considered promising alternatives to lead-based counterparts due to their remarkable optoelectronic properties, which include high absorption coefficients, adjustable bandgaps, and cost-effective manufacturing processes that together improve the utilization and potential of solar energy [3,4,5]. For example, Formamidinium (FA)-based lead-free perovskite solar cells exhibit higher efficiency, greater stability, and reduced toxicity [6]. In addition, tin (Sn)-based PSCs are gaining attention as promising alternatives to their lead (Pb)-based counterparts, offering similar optoelectronic properties such as high carrier mobility, strong light absorption, and long carrier diffusion lengths. Also, they offer significantly lower environmental and health hazards [7].

In recent years, considerable work has been conducted on lead-free PSCs by utilizing various ETL, HTL, and absorber layers. In this context, Ateeq et al used SCAPS simulation to improve performance of $FTO/CeO_2/FASnI_3/CuI/Au$ for a lead-free solar cell by optimizing different values for bandgap, electron affinity, acceptor density, thickness, defect density, and back contact work function [8]. After optimization, the efficiency improved from 22.06% to 24.87%, and the current density increased from 26.03 to 30.68 mA/cm^2. Various hole transport layers (HTLs), including PEDOT:PSS, Spiro-OMeTAD, PCBM, Cu_2O, MoO_3, and Si, have been investigated in perovskite solar cells. In another study, Almufarij et al. optimized a lead-free n-i-p $MASnI_3$ device using graphene, ZnO:Al, and 3C-SiC interface layers, achieving a theoretical efficiency of 30.43% and highlighting $MASnI_3$ as a promising non-toxic material for sustainable energy [9].

On the other hand, ETL materials can be prepared from various materials, such as transition-metal dichalcogenides (TMDCs). ZrS_2 is a two-dimensional (2D) transition metal disulfide synthesized as a thin film for application in flexible transparent devices [10]. Various growth techniques can be employed to achieve tunability of bandgap energy, electronic, and optical properties for ZrS_2 thin films, such as Chemical Vapor Deposition (CVD) and Atomic Layer Deposition (ALD) [11]. It has a high electron mobility and a small energy gap, making it useful for solar cell applications [10]. In this study, we report the optimization of $FASnI_3$ /ZrS_2 solar cells using the SCAPS-1D software [12, 13]. The effects of absorber layer thickness, defect density states, doping density, and the work function of the back metal contact on the performance of $FASnI_3/ZrS_2$ solar cells are investigated.

Cite as: H. Al-Dmour, East Eur. J. Phys. 4, 284 (2025), https://doi.org/10.26565/2312-4334-2025-4-26

2. SIMULATION TOOL

Numerical simulation can play a vital role in optimizing various solar cell structures, such as those using SILVACO, COMSOL, SETFOS, and SCAPS-1D [14]. In this work, the SCAPS-1D simulation was employed to investigate the efficiency of solar cells comprising $FASnI_3$ and ZrS_2. This program was developed by researchers at the University of Gent's Department of Electronics and Information Systems (ELIS), Belgium, for two reasons: to simulate the physical phenomena that occur within the solar cell and to predict how well the solar cell would operate under various conditions, such as differences in temperature, illumination angles, and sun radiation [12]. The program solves Poisson's and continuity equations for free electrons and holes in the conduction and valence bands, which are commonly used in different mechanisms of electronic devices. The equations are given below:

$$\frac{d^2\psi}{dx^2} + \frac{q}{\varepsilon}\left[p(x) - n(x) + N_D - N_A + \rho_p - \rho_n\right] = 0 \tag{1}$$

$$\frac{1}{q}\frac{dJ_P}{dx} = G_{op} - R(x) \tag{2}$$

$$\frac{1}{q}\frac{dJ_n}{dx} = -G_{op} + R(x) \tag{3}$$

Where ε is the dielectric constant, q is the electron charge, N_A and N_D are ionized acceptors and donor density, Ψ is the electrostatic potential, Jp is current density due to hole, Jn is current density due to electron, G_{op} is the carrier generation rate, R is the total recombination rate, p is free hole density, n is the free electron density, ρ_p, and ρ_n are the hole and electron distribution. The following drift-diffusion equations (2) and (3) represent the holes and electrons carrier transport properties of the semiconducting material. The structure of the HTL-free $FASnI_3$-based perovskite solar cell is illustrated in Figure (1).

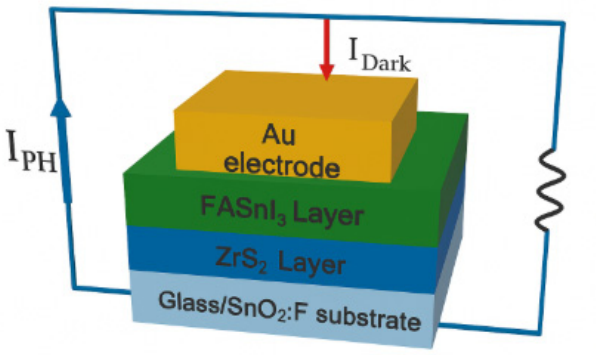

Figure 1. Schematic diagrams of SnO_2:F/ZrS_2/$FASnI_3$ Au solar cells

The figure shows that the proposed solar cell is composed of these layers: $FASnI_3$as absorber material, ZrS_2 as electron transport material (ETL), and two electrodes: gold (Au) as the back contact and fluorine-doped tin oxide (SnO_2:F) as the front contact. The proposed device configurations are developed by modifying the properties of the materials used in this study. Table 1 summarizes the input parameters for HTL-free $FASnI_3$-based perovskite solar cells, as obtained from the literature, to evaluate their performance [11,15]. To establish a stable reference frame for our analysis, we examined the most significant parameters that influence the performance of the tested device. In general, the main unchanged parameters based on published data are the effective density of states at 1×10^{18} cm^{-3} for the valence band and 10^{19} cm^{-3} for the conduction band of these solar cells. For charge carrier behavior at the interfaces, we applied surface recombination velocities of 1×10^5 cm/s for electrons and a slightly higher 10^7 cm/s for holes, reflecting common trends in perovskite materials.

Table 1. Simulation parameters of each layer of the proposed solar cell [11-15].

Parameters	ZrS_2	$FAnSI_3$
Thickness (μm)	Varying 0.2 to 1.4	Varying 0.2 to 2.0
Bandgap (eV)	1.5	1.750
Electron affinity (eV)	4.7	4.125
Dielectric permittivity (relative)	16.4	8.2
CB effective density of states (cm^{-3})	$2.2\times10^{+19}$	1×10^{18}
VB effective density of states (cm^{-3})	$1.8\times10^{+19}$	1×10^{18}
Electron mobility ($cm^2/V\cdot s$)	300	22
Hole mobility ($cm^2/V\cdot s$)	30	22
Shallow uniform donor density ND (cm^{-3})	1×10^{19}	0
Shallow uniform acceptor density NA (cm^{-3})	0	1×10^{16}
Metal work function (eV)	Back contact (Au electrode) 5.1	Front contact (SnO_2:F electrode) 4.4

3. RESULTS AND DISCUSSION

3.1. Effect of Thickness of ZrS_2 Layer and $FAnSI_3$ Layer

The thickness of the components in solar cells plays a vital role in improving their efficiency, as it is a key factor in optimizing solar cells performance. The power conversion efficiency of solar cells depends on the efficiency of photon

absorption, exciton generation, and migration. Solar cells with a thicker layer enhance light absorption and increase charge generation, but they produce a longer path and affect the generation and migration of photo-generated charge carriers. On the other hand, the thinner layers in solar cells may decrease light absorption but facilitate charge-carrier movement. Figure 2 shows the parameters of the $FASnI_3/ZrS_2$ solar cell when the thicknesses of the ZrS_2 and $FASnI_3$ layers were varied from 0.2 µm to 1.4 µm and 0.2 µm to 2.0 µm, respectively.

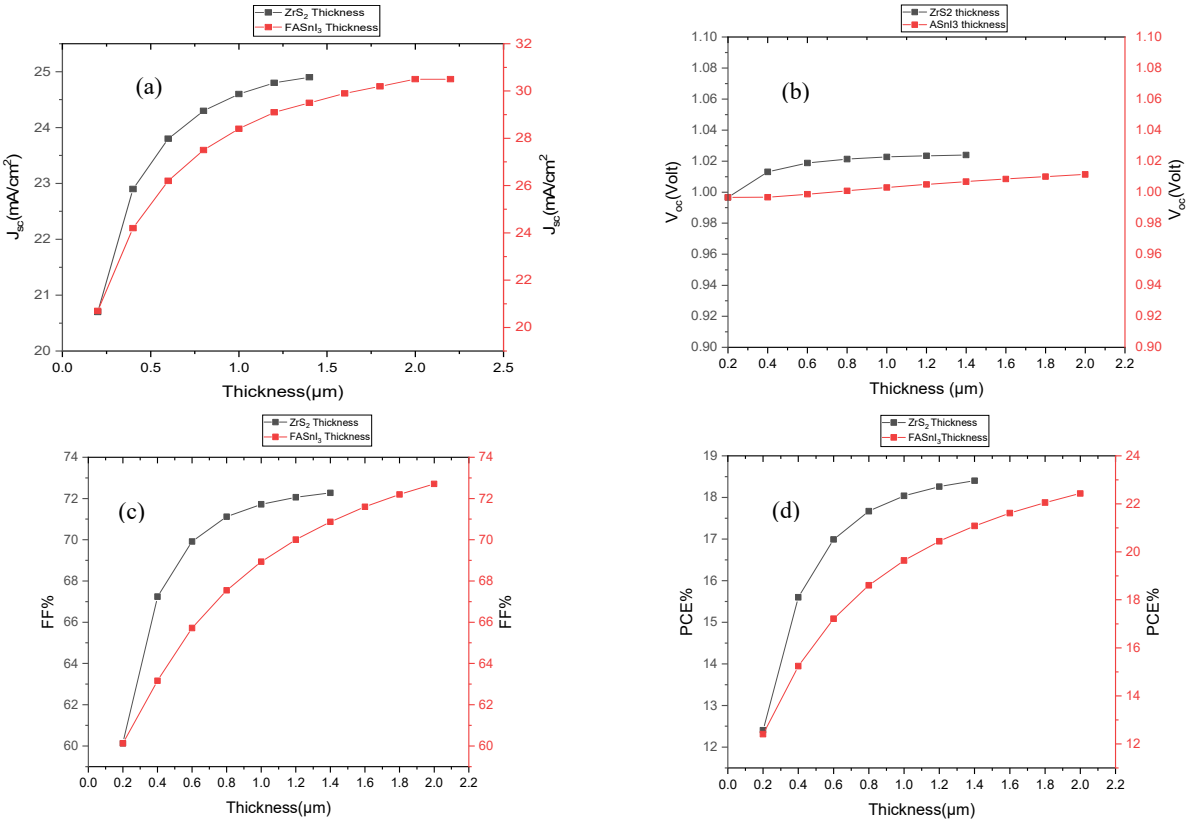

Figure 2. Effect of thickness of ZrS_2 and $FASnI_3$ on the parameters of $ZrS_2/FASnI_3$ solar cells

The results reveal that thinner $FASnI_3$ and ZrS_2 layers produce lower fill factor and PCE compared to their thicker layers in $FASnI_3$ /ZrS_2 solar cells. Figures 2a and 2b show that the short-circuit current density increases (J_{sc}) and reaches its peak value with an increase in thickness, while the open-circuit voltage (Voc) remains constant. However, the J_{SC} gets saturated with minor changes when the thickness of ZrS_2 and $FASnI_3$ changes from 0.8 µm to 1.4 µm and 1.2 µm to 2 µm, respectively. This saturation behavior suggests that beyond these thresholds, additional thickness does not contribute to further light absorption or current generation, likely because most incident photons are already absorbed. On the other hand, the open-circuit voltage (V_{oc}) remained relatively constant across the thickness range studied, as it is more closely governed by the interface recombination rates and energy level alignment between the absorber and transport layers rather than by optical thickness [16]. Moreover, Figures 2c and 2d show that the efficiency (PCE) and fill factor (FF) were enhanced with increasing layer thickness, ranging from 12% to 21.32% and 60% to 72%, respectively. The above results are attributed to improved light absorption in the thicker active layers, which leads to enhancement of photogeneration of charge carriers. Similarly, the increase in FF indicates more efficient charge extraction and minimizes the effect of series resistance.

3.2. Effect of the Total Defect Density in Active Layers and Interfaces

Another essential factor that may significantly impact the device's efficiency is the defect density of the active layers. The level of defect density directly influences the quality of the interface and the bulk body of the solar cells, where the photo-generated charge is transported to the top and bottom electrodes [17,18]. As is known, the source of defect density in electronic devices comes from point defects, stacking faults, dislocations, and grain boundaries, which affect the performance of thin-film solar cells [18]. Additionally, different interfaces are formed in PSCs due to the use of various deposition techniques for each layer. The defects at the interface are influenced by the quality of the materials and the deposition methods, which occur due to interactions between the absorber precursor and the charge transport layer (CTL) solutions, leading to two main types of interface defects: those at the HTL/Perovskite and Perovskite/ETL interfaces. Figure 3 shows the fluctuation in device efficiency with varying defect densities in the ZrS_2 and $FASnI_3$ layers, as well as at the interface between ZrS_2 and $FASnI_3$.

Figure 3-a illustrates the effect of varying the defect density in the ZrS_2 and $FASnI_3$layers on the power conversion efficiency (PCE) of the$FASnI_3/ZrS_2$ solar cell structure. The results show that efficiency remains unchanged when the

defect density is below 1×10^{16} cm^{-3}, but then declines rapidly as the defect density increases from 1×10^{16} cm^{-3} to 10^{20} cm^{-3}. These results are attributed to an increase in the carrier recombination rate in the bulk of the ZrS_2 layer due to deep trap states, which affects the efficient extraction of photo-generated electrons. This leads to a reduction in the diffusion length and the carrier transport lifetime. On the other hand, PCE remains relatively stable with a slight decrease from ~12.5% to ~11% when the defect densities in $FASnI_3$ were varied from 1x $10^{12}cm^{-3}$ to 1x 10^{20} cm^{-3}. That indicates the tendency of the $FASnI_3$ layer to maintain its properties despite the presence of defects that do not affect its lifetimes and transport. That is attributed to defects usually or shallow states that minimally affect carrier recombination. These results align with the findings from the literature, indicating severe degradation in device performance when defect densities in ETLs exceed 1×10^{17} cm^{-3}, while tin-based perovskites maintain reasonable efficiency even under high defect conditions [19]. Figure 3-b shows the fluctuation in device properties with defect density at $ZrS_2/FASnI_3$ interface. As is known, the defects at the interface are influenced by the quality of the materials and the deposition methods occurred due to interactions between the absorber precursor and the charge transport layer (CTL) solutions, leading to two main types of interface defects: those at the HTL/Perovskite and Perovskite/ETL interfaces.

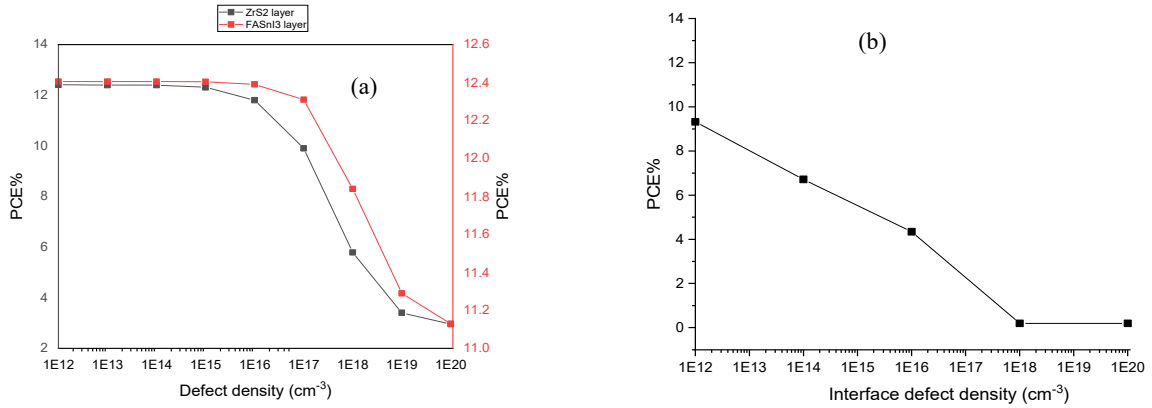

Figure 3. Effect of defect density in a) $ZrS_2$and$FASnI_3$layers and b) ZrS_2/FAS interface on the parameters of $ZrS_2/FASnI_3$ solar cells

3.3. Influence of Doping Densities in ZrS_2 and $FAnSI_3$ Layers

The performance of perovskite and lead-free photovoltaic devices is significantly affected by the doping densities of theZrS_2 and $FAnSI_3$ layers. Figure 4 illustrates the parameters of the $ZrS_2/FAnSI_3$ solar cell as functions of the doping concentration varied from 1×10^{15} to $1\times10^{21}cm^{-3}$

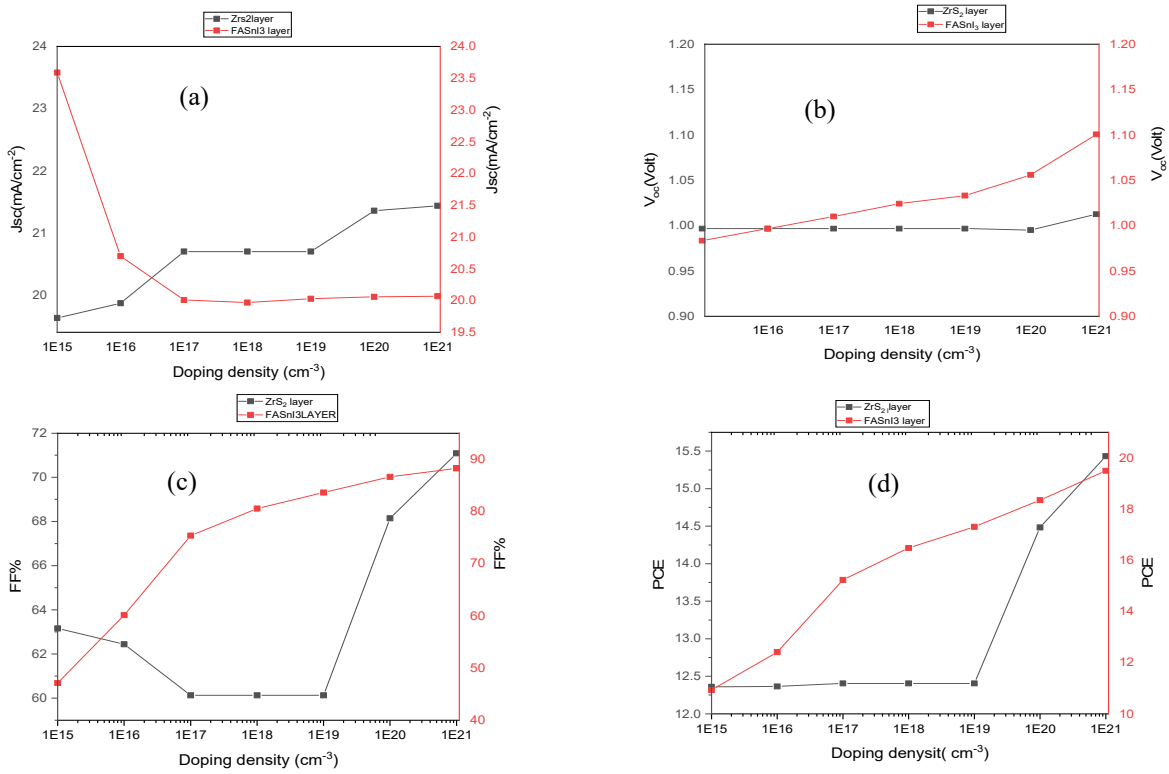

Figure 4. Effect of doping density in ZrS_2 and $FASnI_3$ layers on the parameters of $ZrS_2/FASnI_3$ solar cells

Figures 4a and 4b show a slight enhancement in V_{oc} and J_{sc} as the doping concentration in the ZrS_2 layer increases. For the ZrS_2 layer, PCE increased from 12.4% to 16%, and FF from 54% to 73% (see figures 4c and 4d). These results suggest that heavy doping in the ZrS_2 layer enhances conductivity and charge generation by decreasing the series resistance. On the other hand, the doping density in the $FASnI_3$ absorber had a much more impact on the solar cell performance. The FF improved from 47.12% at the lowest doping level to 88.26% at the highest, while the PCE nearly doubled from 10.93% to 19.50%. That is attributed to several factors: (1) increased built-in electric field strength that facilitates charge separation and collection, (2) reduced carrier recombination due to higher quasi-Fermi level splitting, and (3) improved conductivity and reduced resistive losses in the absorber layer [20,21]. Unlike the ZrS_2 layer, the $FASnI_3$ doping had an immediate and continuous positive effect even at lower doping levels. This confirms that optimizing the absorber layer doping plays a more critical role in achieving high-efficiency solar cell performance.

3.4. Impact of the operating temperature

The operating temperature of perovskite solar cells (PSCs) affects their performance as they are typically installed outdoors and exposed to environmental conditions [22]. Table 2 summarizes the effect of different operating temperatures on the performance of the $FASnI_3/ZrS_2$ solar cells under initial conditions. It is found that V_{OC} decreases from 0.99 to 0.82V while J_{SC} remains relatively constant when the temperature increases from 300K to 420K. The FF varies from 60 % to 64.9 %. Consequently, the power conversion efficiency decreases from approximately 12.2% at 300 K to 11% at 420 K.

Table 2. The parameter of $FASnI_3/ZrS_2$ solar cells as a function of temperature

Temperature (K)	PCE (%)	FF (%)	J_{SC} (mA/cm^2)	V_{OC} (V)
300	12.2	60.12	20.7	0.99
320	12.4	60.26	20.67	0.99
340	12.3	60.88	20.64	0.98
360	12.1	61.97	20.62	0.9
380	11.8	63.15	20.60	0.91
400	11.4	64.14	20.57	0.86
420	11.0	64.92	20.54	0.82

The results reveal that rising temperatures negatively affect solar cell performance, mainly by reducing V_{oc}, $J_{sc,}$ and PCE. This decline is caused by an increase in reverse saturation current density (Jo) due to the increased thermal generation of charge carriers, as explained by the Shockley diode Equation [23]:

$$V_{oc}=\frac{nK_BT}{q}\left[In\left(1+\frac{J_{sc}}{J_o}-\frac{V_{oc}}{J_sR_{sh}}\right]\right. \quad (4)$$

where V_{OC} is the open circuit voltage, n is the ideality factor, K_B is the Boltzmann constant, *J*o is the reverse current, R_{sh} is the shunt resistance, T is the temperature (absolute), and q is the electric charge. The relationship between V_{OC} and Jo is inverse and logarithmic.

Additionally, high temperatures promote recombination by narrowing the semiconductor's energy bandgap, further reducing V_{oc}. According to the literature [23,24], higher temperatures change the properties of the materials used and reduce both the efficiency and V_{oc} of solar cells. This degradation is attributed to a change in the physical and chemical properties of the semiconductor materials used in solar cells. High temperatures break some of the bonds between atoms or molecules in solar cells. These effects reduce the energy gap of materials, change the mobility, and concentrations of charge carriers. Finally, there was a slight reduction in J_{sc}, as charge-separation processing at the interface was also reduced.

3.5 Effect of back-contact work function

In general, the performance of solar cells mainly depends on the alignment of energy levels at the interface between the materials used in fabrication. The properties of interfacial layers between the back and front contact electrodes, as well as the ETL and HTL, play a vital role in achieving high efficiency [25,26]. Figure 5 shows the PCEs of $ZrS_2/FASnI_3$ solar cells as a function of different back-contact work functions. These metals are: Silver (Ag, 4.6 eV), Indium tin oxide (ITO, 4.7eV), Iron (Fe, 4.8eV), Cobalt (Co, 4.9C), Gold (Au, 5.1eV), Tungsten (W, 5.2ev), Nickel (Ni, 5.3) [27]. The PCE curve shows that increasing the back-contact work function from 4.6 eV to 5.3 eV increases PCE from 6.7% to 13.1%. That depends on the properties of the interfacial contact between the metals and the $FASnI_3$ layers, which are determined by the chemical interaction between them. Metals with high work functions (W and Ni) form near-ohmic contacts with the $FASnI_3$ layer, consequently facilitating hole extraction and producing high PCE. In contrast, metals with lower work functions, such as Ag and ITO, produce low PCE due to forming in Schottky barriers that hinder hole extraction. These results emphasize that better energy-level alignment at the metal (work function > 5eV) /$FASnI_3$ interface enhances charge-carrier extraction and overall solar cell efficiency.

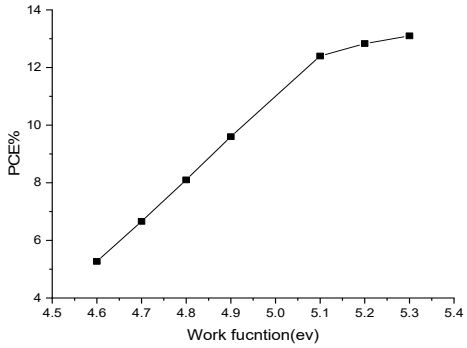

Figure 5. The PCE of $FASnI_3/ZrS_2$ solar cells as a function of the work function of the back contact

3.6 Device optimization

Optimal device performance is achieved by optimizing various variables of the solar cells. Figure 6 illustrates the difference in the current-voltage characteristics of optimized and non-optimized solar cells.In this work, an optimization route is presented that significantly enhances the efficiency of $FASnI_3/ZrS_2$ solar cells, offering an essential reference for further development of high-performance photovoltaic devices. After optimization, the open-circuit voltage (VOC) was adjusted from 0.99 V to 0.93 V, while the short-circuit current density (JSC) increased from 20.7 mA/cm² to 30.2 mA/cm². This was accompanied by an improvement in the fill factor (FF) from 60.1% to 82.4%, leading to an enhancement in the power conversion efficiency (PCE) from 12.4% to 23.3%. These enhancements are attributed to increasing the thickness of the $FASnI_3$ absorber layer from 0.2µm to 1.5µm, which improves photon absorption, generates more electron-hole pairs, and increases the short-circuit current density. Additionally, the ZrS_2 electron transport layer thickness was modified to 1.0 µm, which facilitated more efficient electron extraction and minimized recombination losses at the interface. A significant increase in the acceptor doping concentration of both $FASnI_3$ and ZrS_2 – from 1×10^{17} cm^{-3} to 1×10^{21} cm^{-3} – strengthened the built-in electric field across the junction, enhancing charge carrier separation and reducing resistive losses. Finally, increasing the back contact work function to 5.3 eV optimized the energy level alignment, improving hole collection and suppressing recombination at the rear interface

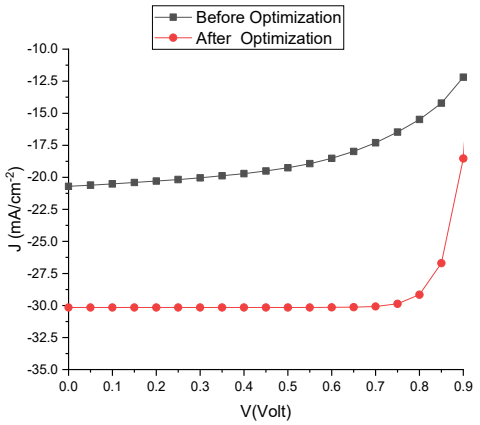

Figure 6. J-V curves before and after optimization

4. CONCLUSIONS

This study successfully demonstrated the numerical optimization of lead-free $FASnI_3/ZrS_2$ perovskite solar cells using SCAPS-1D simulation. By systematically varying key parameters such as layer thickness, defect density, doping concentration, operating temperature, and back-contact work function, the device performance was significantly enhanced. The optimized solar cell achieved a remarkable power conversion efficiency of 23.3%, with improved open-circuit voltage, short-circuit current, and fill factor compared to the initial design. The improvements are mainly attributed to increased thickness and doping density of the absorber and electron transport layers, as well as better energy alignment through a higher back-contact work function. These results provide valuable guidance for developing efficient and environmentally friendly lead-free perovskite solar cells.

Acknowledgements

The authors are thankful to Prof. Marc Burgelman of the University of Gent, Belgium, for providing the SCAPS 1D software for their studies.

ORCID

Hmoud Al-Dmour, https://orcid.org/0000-0001-5680-5703

REFERENCES

[1] J. Zhang, Geosci. Front. 15(5), 101873 (2024). https://doi.org/10.1016/j.gsf.2024.101873
[2] M.S. Reza, A. Ghosh, N. Drissi, H. Al-Dmour, R.K. Prodhan, M.M. Islam, S. Begum, *et al*., RSC Adv. **14**, 36675 (2024). https://doi.org/10.1039/D4R07912D
[3] A.S. Abdulkarim, M. Srivastava, T. Ngulezhu, D. Singh, K. Strzałkowski, R.C. Singh, M.Z.A. Yahya, *et al*., Curr. Appl. Phys. **71**, 190 (2025). https://doi.org/10.1016/j.cap.2024.12.025
[4] A. Kojima, K. Teshima, Y. Shirai, and T. Miyasaka, J. Am. Chem. Soc. **131**(17), 6050 (2009). https://doi.org/10.1021/ja809598r
[5] M. Tarekuzzaman, N. Shahadat, M. Montasir, O. Alsalmi, M.H. Mia, H. Al-Dmour, M. Rasheduzzaman, and M.Z. Hasan, RSC Adv. **15**, 13643 (2025). https://doi.org/10.1039/D5RA01748C
[6] K. Sekar, L. Marasamy, S. Mayarambakam, H. Hawashin, M. Nour, and J. Bouclé, RSC Adv. **13**, 25483 (2023). https://doi.org/10.1039/D3RA04617D
[7] A. Yadegarifard, H. Lee, H.-J. Seok, I. Kim, B.-K. Ju, H.-K. Kim, and D.-K. Lee, Nano Energy, **112**, 108481 (2023). https://doi.org/10.1016/j.nanoen.2023.108481
[8] A. Rehman, S. Afzal, I. Naeem, D. Bibi, S.G. Sarwar, F. Nabeel, and R.M. Obodo, Hybrid Adv. **7**(2), 100301 (2024). https://doi.org/10.1016/j.hybadv.2024.100301
[9] S.A.A. Jafri, R.S. Almufarij, A. Ashfaq, R.S. Alqurashi, L.G. Alharbe, A.R. Abd-Elwahed, O.A. Albeydani, *et al*., Sol. Energy, **270**, 112391 (2024). https://doi.org/10.1016/j.solener.2023.112391
[10] H. Al-Dmour, East Eur. J. Phys. (2), 445 (2024). https://doi.org/10.26565/2312-4334-2024-2-58
[11] M. Abdelfatah, A. El-Sayed, W. Isamil, V. Sittinger, and A. El-Shaer, Sci. Rep. **13**, 4553 (2023). https://doi.org/10.1038/s41598-023-31553-4
[12] M. Burgelman, P. Nollet, and S. Degrave, Thin Solid Films, **361-362**, 527 (2000). https://doi.org/10.1016/S0040-6090(99)00825-1
[13] B. Zaidi, N. Mekhaznia, M.S. Ullah, and H. Al-Dmour, J. Phys.: Conf. Ser. **2843**, 012012 (2024). https://doi.org/10.1088/1742-6596/2843/1/012012
[14] A. Das, S.D. Peu, M.A.M. Akanda, M.M. Salah, M.S. Hossain, and B.K. Das, Energies, **16**, 2328 (2023). https://doi.org/10.3390/en16052328
[15] A. Rehman, S. Afzal, I. Naeem, D. Bibi, S.G. Sarwar, F. Nabeel, and R.M. Obodo, Hybrid Adv. **7**, 100301 (2024). https://doi.org/10.1016/j.hybadv.2024.100
[16] O.J. Sandberg, A. Sundqvist, M. Nyman, and R. Österbacka, Phys. Rev. Appl. **5**, 044005 (2016). https://doi.org/10.1103/PhysRevApplied.5.044005
[17] H. Al-Dmour, and D.M. Taylor, J. Ovonic Res. **19**(5), 587 (2023). https://doi.org/10.15251/JOR.2023.195.587
[18] L. Zhao, J. Schmidt, and A. Cuevas, Appl. Phys. Lett. **101**, 123904 (2012). https://doi.org/10.1063/1.4754609
[19] H. Karmaker, A. Siddique, B.K. Das, and M.N. Islam, Results Eng. **22**, 102106 (2024). https://doi.org/10.1016/j.rineng.2024.102106
[20] G.G. Njema, B.C. Mosonik, C.C. Ahia, and J.K. Kibet, Chem. Eur. J. **30**(71), e202403192 (2024). https://doi.org/10.1002/chem.202403192
[21] H. Al-Dmour, AIMS Mater. Sci. **8**(2), 261 (2021). https://doi.org/10.3934/matersci.2021017
[22] S. Wu, C. Li, S.Y. Lien, and P. Gao, Chemistry, **6**, 207 (2024). https://doi.org/10.3390/chemistry6010010
[23] D.W. Husainat, P. Ali, J. Cofie, J. Attia, A. Fuller, and A. Darwish, AJOP, **8**(1), 6 (2020). https://doi.org/10.11648/j.ajop.20200801.12
[24] T. Rahman, A.A. Mansur, M.S.H. Lipu, *et al*., Energies, **16**(9), 3706 (2023). https://doi.org/10.3390/en16093706
[25] G.G. Njema, J.K. Kibet, S.M. Ngari, Measurement: Energy, **2**, 100005 (2024). https://doi.org/10.1016/j.meaene.2024.100005
[26] M.A. Madanat, A.A. Al-Tabbakh, M. Alsa'eed, H. Al-Dmour, and M.S. Mousa, Ultramicroscopy, **234**, 113479 (2022). https://doi.org/10.1016/j.ultramic.2022.11347
[27] A. Kumar, N.P. Singh, A. Sundaramoorthy, Mater. Lett. X, **12**, 100092 (2021). https://doi.org/10.1016/j.mlblux.2021.100092

ЧИСЛОВЕ ДОСЛІДЖЕННЯ БЕЗСВИНЦЕВИХ ПЕРОВСКИТНІХ СОНЯЧНИХ ЕЛЕМЕНТІВ НА ОСНОВІ СТРУКТУРИ $FASnI_3/ZrS_2$ ЗА ДОПОМОГОЮ СИМУЛЯТОРА SCAPS-1D

Хмуд Аль-Дмур
Університет Мута, факультет природничих наук, кафедра фізики, 61710, Йорданія

У цьому дослідженні представлено чисельне дослідження та оптимізацію сонячних елементів на основі безсвинцевого перовскіту за допомогою моделювання SCAPS-1D. Запропонований пристрій складається з йодиду формамідинію-олова ($FASnI_3$, поглинаючий шар), дисульфіду цирконію (ZrS_2, матеріал для переносу електронів), золота (Au, задній контакт) та легованого фтором оксиду олова (SnO_2:F, передній контакт). Було досліджено вплив зміни товщини, щільності дефектів, концентрації легування, робочої температури та роботи виходу заднього контакту на характеристики фотоелектричної системи з метою визначення оптимальної архітектури пристрою з найвищою ефективністю перетворення енергії (PCE). Результати показують, що початкова продуктивність сонячних елементів $FASnI_3/ZrS_2$ була наступною: напруга холостого ходу (VOC) = 0,99 В, струм короткого замикання (JSC) = 20,7 мА/см^2, коефіцієнт заповнення (FF) = 60,13% та коефіцієнт перетворення потужності (PCE) = 12,4%. Після оптимізації продуктивність $FASnI_3/ZrS_2$ значно покращилася, досягнувши PCE 23,3%, FF 82,4% та JSC 30,2 мА/см². Це помітне покращення цих параметрів пояснюється збільшенням товщини та щільності легування шарів $FASnI_3$ та ZrS_2, що призводить до покращеного поглинання світла та генерації заряду. Крім того, було виявлено, що робота виходу зворотного контакту 5,3 еВ створює краще узгодження енергетичних рівнів із шаром $FASnI_3$, що сприяє вилученню заряду. Ці результати пропонують цінну інформацію про розробку ефективних, стабільних та безсвинцевих перовскітних сонячних елементів.

Ключові слова: *$FASnI_3$; ZrS_2; SCAPS-1D; безсвинцеві перовскітні сонячні елементи; шар електрон-транспорту; фотоелектричне моделювання; сонячна енергія*